



Melatonin loaded nanostructured lipid carriers for the treatment of uveal melanoma

Lorena Bonilla-Vidal^{a,b}, Marta Espina^{a,b}, María Luisa García^{a,b}, Cinzia Cimino^{c,d,e},
Claudia Carbone^{d,e}, Laura Baldomà^{f,g}, Josefa Badia^{f,g}, Anna Gliszczynska^h, Eliana B. Soutoⁱ,
Elena Sánchez-López^{a,b,*}

^a Department of Pharmacy, Pharmaceutical Technology and Physical Chemistry, University of Barcelona, 08028, Barcelona, Spain

^b Institute of Nanoscience and Nanotechnology (IN²UB), University of Barcelona, 08028, Barcelona, Spain

^c Department of Biomedical and Biotechnological Sciences, University of Catania, Via Santa Sofia 97, 95123, Catania, Italy

^d Laboratory of Drug Delivery Technology, Department of Drug and Health Sciences, University of Catania, Viale A. Doria 6, 95124, Catania, Italy

^e NANOMED, Research Centre for Ocular Nanotechnology, University of Catania, Italy

^f Department of Biochemistry and Physiology, University of Barcelona, 08028, Barcelona, Spain

^g Institute of Biomedicine of the University of Barcelona (IBUB), Institute of Research of Sant Joan de Déu (IRSJD), 08950, Barcelona, Spain

^h Department of Food Chemistry and Biocatalysis, Wrocław University of Environmental and Life Sciences, Norwida 25, 50-375, Wrocław, Poland

ⁱ UCD School of Chemical and Bioprocess Engineering, University College Dublin, Belfield, Dublin 4 D04 V1W8, Ireland

ARTICLE INFO

Keywords:

Drug delivery
Nanostructured lipid carriers
Melatonin
Uveal melanoma
Anti-inflammatory efficacy
Cytotoxicity studies

ABSTRACT

Uveal melanoma, a highly aggressive intraocular tumor and the second most common form of ocular malignancy, currently lacks effective therapeutic options. Therefore, this study addresses an unmet medical need by developing nanostructured lipid carriers (NLC) as a potential delivery system for melatonin (MEL) to target uveal melanoma. NLC were optimized for ophthalmic administration by the addition of a cationic surfactant to increase mucoadhesivity to the negatively charged ocular surface. MEL-loaded NLC (MEL-NLC) exhibited suitable particle size (<200 nm), good colloidal stability (5 months), and sustained MEL release. *In vitro* cytotoxicity assays demonstrated antiproliferative activity against uveal melanoma cells while maintaining corneal cell viability, further confirmed by *in vitro* HET-CAM test and *in vivo* ocular tolerance studies. Additionally, inflammation studies were performed since inflammation constitutes one of the main hallmarks of cancer development and progression. Consequently, MEL-NLC displayed anti-inflammatory properties. Furthermore, preliminary biodistribution results suggested their ability to reach the posterior segment of the eye, mainly the retina and the ciliary body, positioning them as a promising strategy for uveal melanoma treatment.

1. Introduction

Uveal melanoma (UM) is the second most common type of primary ocular malignancy, with an incidence ranging from 0.1 to 8.6 cases per million individuals. It is particularly prevalent among individuals of Caucasian descent and its incidence also increases with age, with the majority of cases occurring in individuals over 50 years old. Despite its relative rarity, UM is a highly aggressive cancer that poses significant challenges due to the lack of effective therapeutic options [1]. UM originates from melanocytes residing in the uvea, a pigmented layer of the eye comprising the iris (in the front chamber), choroid, and ciliary body. More than 90 % of UM develops in the choroid, while only 6 %

occurs in the ciliary body and 4 % involve the iris [2,3]. Ocular treatment primarily aims to preserve vision and the eye itself, encompassing a diverse range of therapies including radiotherapy, phototherapy, and local resection, with enucleation reserved for exceptionally severe cases [4]. Despite extensive research efforts, the overall survival rate of patients with metastatic UM has remained stagnant over the past three decades. Even following successful treatment of the primary tumor, approximately 50 % of UM patients develop a metastatic disease, which typically disseminates in a heterogeneous manner. Currently, there are no effective therapies to prevent metastasis, but a rapid intervention may potentially prevent the development of lethal UM. Metastases from UM exhibit limited responsiveness to chemotherapy or targeted therapy

* Corresponding author. Department of Pharmacy, Pharmaceutical Technology and Physical Chemistry, University of Barcelona, 08028, Barcelona, Spain
E-mail address: esanchezlopez@ub.edu (E. Sánchez-López).

and are typically fatal within one year of their appearance [1,3,5].

Melatonin (MEL), a ubiquitously expressed endogenous molecule, is primarily produced by the pineal gland, intestinal tract, immune system, and brain. Beyond its role in regulating circadian rhythms, MEL exhibits a broad spectrum of biological activities, influencing endocrine processes, reproductive cycles, bone metabolism, cell cycle progression, and mitochondrial function regulation [6]. Notably, MEL possesses oncogenic properties, demonstrating promising potential as an anti-cancer therapeutic agent in various malignancies. Studies conducted on UM and normal uveal melanocyte cell lines have suggested MEL selective ability to suppress the growth of UM cells while sparing normal melanocytes. Additionally, cell culture and animal model studies have provided evidence that MEL can inhibit the proliferation of both uveal and cutaneous melanoma cells. In UM patients undergoing plaque brachytherapy, MEL's antioxidant properties may offer additional benefits by counteracting the detrimental ocular side effects associated with radiation exposure [7,8]. Despite its promising properties, MEL is degraded when exposed to air and light. Studies have shown that MEL's half-life is significantly reduced when exposed to these conditions [9]. This degradation can lead to reduced effectiveness of MEL as a therapeutic agent.

In last decades, different nanocarriers with sustained drug delivery capabilities have been developed for ocular applications. These nanoscale delivery systems present few advantages in comparison to traditional drug delivery methods for treating posterior eye diseases, such as their ability to effectively target specific ocular tissues and release medication over an extended period [10,11]. Nanotechnology has the potential to improve oncology by providing innovative approaches for cancer therapy, detection, and diagnosis. This field offers the possibility of directly targeting chemotherapeutic agents to cancerous cells and tumors, guiding surgical resection, and enhancing the therapeutic efficacy of radiation and other existing treatment modalities [12,13]. Among various types of nanoparticles (NP), lipid NP have gained considerable attention owing to their ease of scale-up and low toxicity. Solid lipid nanoparticles (SLN), the first-generation lipid NP, emerged in the early 1990s. While demonstrating promising results, they exhibited limitations such as drug expulsion during storage and limited drug loading capacity. To address these shortcomings, nanostructured lipid carriers (NLC), the second-generation lipid NP, emerged. By incorporating liquid lipids into the formulation, NLC enhanced the cargo capacity of NP and improved storage stability [14–16].

Previous studies have demonstrated the potential of NLC encapsulating MEL using natural compounds as a suitable delivery system to potentially treat several types of tumors [17]. Therefore, we aimed to develop a novel formulation, MEL-NLC, designed to protect MEL from degradation and extend its short half-life, incorporating a cationic surfactant, dimethyldioctadecylammonium bromide (DDAB), in order to enhance the bioavailability of NLC when administered onto the ocular mucosa. Cationic surfactants, due to their positive charge, exhibit electrostatic attraction with the negatively charged ocular mucosa. This interaction leads to prolonged drug residence time on the ocular surface [18]. Furthermore, DDAB has a well-established safety profile in other studies for ocular delivery, demonstrating no toxicity up to a concentration of 0.5 %, in comparison to other cationic surfactants such as cetyltrimethylammonium bromide [19]. Moreover, in our previous studies using DDAB as a cationic surfactant, the formulation showed *in vitro* safety in human corneal cells, and *in vivo* ocular safety when administered into rabbit eyes [20].

This investigation aimed to optimize a nanostructured drug delivery system utilizing cationic NLC loaded with MEL for the therapeutic management of UM. This study focused on the different *in vitro* and *in vivo* studies to assess their biocompatibility, cytotoxicity against UM cell lines, and anti-inflammatory efficacy to mitigate the inflammation related to cancer [21].

2. Materials and methods

2.1. Materials

MEL was sourced from Thermo Fisher Scientific (Massachusetts, USA). Gattefossé (Madrid, Spain) provided Compritol® 888 ATO (glyceryl distearate). Sigma Aldrich (Madrid, Spain) supplied Tween® 80 (Polysorbate 80) and Nile red (NR). Rosehip oil was obtained from Acofarma Fórmulas Magistrales (Barcelona, Spain), and DDAB from TCI Europe (Zwijndrecht, Belgium). All other reagents were of analytical grade. Water purification was achieved using a Millipore Milli-Q Plus system.

2.2. MEL-NLC preparation and optimization

The preparation of MEL-NLC was performed using the hot high-pressure homogenization technique (Homogenizer FPG 12800, Stanssted, United Kingdom). First, an initial emulsion was obtained by mixing the components at 8000 rpm for 30 s using an Ultraturrax® T25 (IKA, Germany). The fabrication conditions were 85 °C, three homogenization cycles, and a pressure of 900 bar. In order to obtain a positive surface charge, increasing amounts of cationic lipid DDAB were incorporated into the optimized formulation derived from previous studies (data not shown).

2.3. Physicochemical characterization

The physicochemical characteristics of mean average size (Z_{av}) and polydispersity index (PI) were assessed using photon correlation spectroscopy (PCS) with a Zetasizer NanoZS instrument (Malvern Instruments, Malvern, UK). Measurements were conducted at 25 °C and a scattering angle of 90°. Samples were diluted 1:10 with Milli-Q water. Zeta potential (ZP) was determined by electrophoretic light scattering using the same instrument. Samples were diluted 1:20 with Milli-Q water to ensure optimal measurement conditions. All measurements were performed in triplicate to ensure data reproducibility [22,23].

Encapsulation efficiency (EE) was indirectly determined by quantifying the free drug content in the MEL-NLC dispersion [23]. Each sample was centrifuged using Amicon® Ultra 0.5 centrifugal filter device (Amicon Millipore Corporation, Ireland) at 14000 rpm for 15 min. The supernatant contained free MEL, which was quantified by high-performance liquid chromatography (HPLC). EE was determined by calculating the difference between the initial drug quantity and the amount of free drug remaining in the supernatant after centrifugation, using Eq. (1) [24]:

$$EE = \frac{\text{Total amount of MEL} - \text{Free amount of MEL}}{\text{Total amount of MEL}} \times 100 \quad \text{Equation 1}$$

The quantification of MEL was carried out employing a Kromasil® C18 column (5 µm, 150 × 4.6 mm) with a mobile phase gradient. The gradient consisted of a water phase containing 2 % acetic acid and an organic phase constituted by methanol. The gradient eluted from 40 % to 60 % water phase over 5 min and returned to the initial composition in the following 5 min. The flow rate was set at 0.9 mL/min. Detection of MEL was achieved using a Waters® 2996 diode array detector at 300 nm, and data processing was performed with Empower® 3 Software [25].

2.4. Characterization of optimized MEL-NLC

2.4.1. Transmission electron microscopy

The morphology of the NLC was studied by transmission electron microscopy (TEM) on a JEOL 1010 microscope (Akishima, Japan). To visualize the morphology of MEL-NLC, negative staining was employed. Uranyl acetate (2 %) was applied to copper grids previously activated with UV light [26].

2.4.2. Interaction studies

Differential scanning calorimetry (DSC) was employed to analyse the thermal profile of MEL-NLC. DSC 823e System (Mettler-Toledo, Barcelona, Spain) was utilized. System calibration was verified using an indium pan (purity $\geq 99.95\%$; Fluka, Switzerland), and an empty pan served as reference. Measurements were conducted within a nitrogen atmosphere with a heating ramp from 25 to 105 °C at 10 °C/min. Data analysis was performed using Mettler STARE V 9.01 dB software (Mettler-Toledo, Barcelona, Spain) [27].

The crystallinity of the samples was assessed using X-ray diffraction (XRD). Samples were positioned between 3.6 μm polyester films and irradiated with CuK α radiation (45 kV, 40 mA, $\lambda = 1.5418 \text{ \AA}$) in the 2 θ range of 2°–60° with a step size of 0.026° and a dwell time of 200 s per step [28].

Fourier-transform infrared (FTIR) analysis of MEL-NLC was performed using a Thermo Scientific Nicolet iZ10 spectrometer equipped with an ATR diamond and a DTGS detector (Barcelona, Spain) [26].

2.5. Stability studies

MEL-NLC samples were stored at 4, 25, and 37 °C for several months. The stability of these samples was evaluated by analysing their light backscattering (BS) profile using a Turbiscan® Lab instrument. A glass cell containing 10 mL of sample was employed. Data were collected at 30-day intervals. The light source employed was a pulsed near-infrared light-emitting diode ($\lambda = 880 \text{ nm}$), and the BS signal was received by a detector placed at an angle of 45° relative to the incident beam. Simultaneously, Z_{av} , PI, ZP, and EE values were determined [24].

2.6. Biopharmaceutical behaviour

To study the *in vitro* release profile of MEL from the NLC in comparison with free MEL, the direct dialysis method under sink conditions for 48 h was performed ($n = 3$). 9 mL of each formulation were loaded into separated dialysis bags (cellulose membrane, 12–14 kDa MWCO, 3.20/32" diameter, Iberlabo). The bags were then immersed in phosphate-buffered saline (PBS, 0.1 M) containing 0.1 % sodium dodecyl sulphate at pH 7.4 (release media) at 37 °C (body temperature). At predetermined intervals, 0.3 mL aliquots of the release media were withdrawn and replaced with fresh media. MEL concentration in the collected samples was quantified by HPLC, and the data were subsequently analysed using various kinetic models [22,25].

2.7. Ocular tolerance

2.7.1. *In vitro* study: HET-CAM test and HET-CAM TBS

The HET-CAM assay was used to evaluate the *in vitro* ocular tolerance of MEL-NLC formulations, ensuring their suitability for ophthalmic administration [29]. Following Interagency Coordinating Committee on the Validation of Alternative Methods (ICCVAM) guidelines, 300 μL of each formulation (free MEL, MEL-NLC, positive control of NaOH 0.1 M, and negative control of NaCl 0.9 %) were applied to the chorioallantoic membrane of fertilized chicken eggs (3 eggs per group). Each egg was monitored for 5 min post-application, noting the onset of irritation, coagulation, and hemorrhage [30]. The ocular irritation index (OII) was calculated using Eq. (2):

$$OII = \frac{(301 - H) \cdot 5}{300} + \frac{(301 - V) \cdot 7}{300} + \frac{(301 - C) \cdot 9}{300} \quad \text{Equation 2}$$

where H, V, and C represent time (in seconds) until the onset of hemorrhage, vasoconstriction, or coagulation, respectively. Formulations were then classified as: non-irritating ($OII \leq 0.9$), weakly irritating ($0.9 < OII \leq 4.9$), moderately irritating ($4.9 < OII \leq 8.9$), or irritating ($8.9 < OII \leq 21$).

Furthermore, at the end of the HET-CAM experiment, in order to

quantify the damage of the membrane, trypan blue staining (TBS) was applied. Following topical exposure, the chorioallantoic membrane (CAM) was incubated with 1 mL of 0.1 % TBS for 1 min. Dye excess was removed by rinsing with distilled water. The stained CAM was then excised and homogenized in 5 mL formamide. The absorbance of the extract was measured spectrophotometrically at 595 nm to quantify the incorporated trypan blue. A calibration curve of TBS in formamide was used to determine the amount of absorbed dye [31].

2.7.2. *In vivo* study: Draize test

To validate the findings from the HET-CAM assay, the Draize primary eye irritation test was conducted on New Zealand albino rabbits. Firstly, 50 μL of each formulation were instilled into the conjunctival sac of each rabbit ($n = 3/\text{group}$) with a gentle massage to ensure corneal penetration. Signs of irritation (corneal opacity, conjunctival hyperaemia, chemosis, ocular discharge, and iris abnormalities) were monitored immediately, 1 h post-instillation, and at predetermined intervals (24 h, 48 h, 72 h, 7 days, and 21 days). The untreated contralateral eye served as the negative control. Draize scores were assigned based on direct observation of corneal opacity/cloudiness, iris changes, and conjunctival alterations (hyperaemia, chemosis, swelling, and discharge) [27].

2.8. Cellular experiments

2.8.1. Cell culture

Human corneal epithelial (HCE-2) cells were cultured in keratinocyte serum-free growth medium (SFM; Life Technologies, Invitrogen, GIBCO®, Paisley, UK). The medium was supplemented with bovine pituitary extract (0.05 mg/mL), epidermal growth factor (5 ng/mL) containing insulin (0.005 mg/mL), penicillin (100 U/mL), and streptomycin (100 mg/mL). Cells were cultured in flasks at 37 °C in a humidified atmosphere with 10 % CO₂ until reaching 80 % confluency [30].

Human uveal melanoma (UM 92–1) cells were cultured in RPMI-1640 medium (Euroclone, Milan, Italy), added with 10 % fetal bovine serum, 2 mM L-glutamine, 100 U/mL penicillin and 100 $\mu\text{g}/\text{mL}$ streptomycin. Cells were incubated on a culture flask up to 80 % confluency at 37 °C and 10 % CO₂ [32].

2.8.2. Cell viability

The cytotoxicity of MEL-NLC was assessed using the MTT (3-(4,5-dimethylthiazol-2-yl)-2,5-diphenyltetrazolium bromide) assay. This assay measures the metabolic activity of viable cells through the reduction of the tetrazolium salt by intracellular dehydrogenases. For this, 100 μL of a cell suspension of 2×10^5 cells/mL for HCE-2, or 1×10^4 cells/mL for UM 92–1 cells, were seeded in a 96-well plate and incubated for 48 h at 37 °C in the appropriate complete medium before treatment. To mimic real corneal conditions, HCE-2 cells were exposed to various sample concentrations (1×10^{-3} –0.1 mg/mL) for 5, 15, or 30 min, while UM 92–1 cells were incubated for 24 h. Following incubation, the medium was discarded, and a solution of MTT (0.25 % in PBS, Sigma-Aldrich Chemical Co., St. Louis, MO, USA) was added. After a 2-h incubation, the medium was replaced with 100 μL DMSO (99 % dimethyl sulfoxide, Sigma-Aldrich). Cell viability was then quantified by measuring absorbance at 560 nm using a Modulus® Microplate Photometer (Turner BioSystems Inc., Sunnyvale, CA, USA). The results were expressed as the percentage of viable cells compared to untreated control cells [28,30,33].

2.8.3. Cellular uptake

To assess MEL-NLC internalization within HCE-2 cells, 1×10^5 HCE-2 cells/mL were seeded into an eight-well chamber slide (ibidi®, Gräfelfing, Germany) until 80 % confluence. Cells were then incubated with NR labeled MEL-NLC at 37 °C for 5, 15, and 30 min. PBS washes removed non-internalized NLC, followed by fixation with 4 % paraformaldehyde (30 min, 25 °C). After additional PBS washes, nuclei were stained with 4',6-diamidino-2-phenylindole (DAPI) during 10 min at

25 °C, cell membranes with Alexa Fluor™ 488 conjugated Wheat Germ Agglutinin (WGA, 30 min, 25 °C). Images were captured using a Leica Thunder Imager DMI8 (Leica Microsystems GmbH, Wetzlar, Germany) equipped with a 63x oil immersion objective lens [34,35].

2.9. In vivo studies

2.9.1. Anti-inflammatory efficacy

To evaluate MEL-NLC ability to mitigate ocular inflammation, both preventative and anti-inflammatory efficacy tests were conducted on New Zealand male albino rabbits (n = 3/group). Formulations included MEL-NLC, free MEL, and NaCl 0.9 % (control).

For the prevention study, 50 µL of each formulation was applied to the rabbit's eye. After 30 min, 50 µL of 0.5 % sodium arachidonate (SA) in PBS was instilled to induce inflammation (right eye), with the left eye serving as control. In the anti-inflammatory study, SA was applied 30 min before the formulation. Ocular evaluations were performed from initial application to 210 min following a modified Draize scoring system [29,30].

2.9.2. Ocular in vivo biodistribution

In vivo biodistribution studies were conducted by administering two separate 50 µL doses of either MEL-NLC loaded with NR or NR solution into the conjunctival sac of New Zealand albino rabbits, separated by 5 min of clearance. After 3 h, the animals were euthanized, and the eyes were enucleated. Each eye was then immersed in 4 % paraformaldehyde in PBS for 24 h and then transferred to a solution containing 4 % paraformaldehyde and 30 % sucrose. After another 24 h, the eyes were embedded in O.C.T. compound cryo-embedding medium and frozen at -80 °C. Subsequently, frozen eyes were sliced using a cryostat (Leica CM 3050 S, Leica Microsystems GmbH, Wetzlar, Germany) and the cellular nuclei were stained with DAPI to visualize cell structures. Fluorescence images were acquired using a Leica Thunder Imager DMI8 (Leica Microsystems GmbH, Wetzlar, Germany) and analysed using ImageJ software [36].

2.10. In vivo experimentation

All procedures adhered to the guidelines of the UB Ethical Committee for Animal Experimentation and followed current regulations (Decree 214/97, Gencat) and protocols were approved under the code 326/19. Furthermore, all the *in vivo* procedures comply with the ARRIVE guidelines and were carried out in accordance with the U.K. Animals (Scientific Procedures) Act, 1986 and associated guidelines, EU Directive 2010/63/EU for animal experiments.

New Zealand white male rabbits (2–2.5 kg, San Bernardo farm, Navarra, Spain) were kept in individual cages with free access to food and water in a controlled 12/12 h light/dark cycle under veterinary supervision. Rabbits were anesthetized with intramuscular administration of ketamine HCl (35 mg/kg) and xylazine (5 mg/kg) and euthanized by an overdose of sodium pentobarbital (200 mg/kg).

2.11. Statistical analysis

Statistical analyses were conducted using GraphPad Prism 9. Two-way ANOVA followed by Tukey's post-hoc test was used for multiple group comparisons, while Student's t-test was used for pairwise comparisons. Data are presented as mean ± standard deviation (SD). Statistical significance was set at $p < 0.05$.

3. Results

3.1. MEL-NLC preparation and optimization

The optimized formulation obtained in a previous study was used for the present investigation (7.5 % lipid phase, 5 % surfactant, and 0.05 %

MEL). Based on this formulation, increasing amounts of the cationic lipid DDAB were added to study its influence on the physicochemical properties of the nanoparticles (Table 1). The optimized formulation was selected based on the physicochemical parameters, aiming to obtain ZP values greater than +15 mV and PI below 0.3. Following these criteria, the cationic optimized formulation was the one containing 0.07 % of DDAB.

3.2. Characterization of optimized MEL-NLC

TEM analysis revealed that MEL-NLC exhibited almost spherical and soft morphologies (Fig. 1A and B), with particle sizes below 200 nm, corroborating the findings obtained by PCS (Fig. 1C). Moreover, as predicted by the obtained ZP values (+20 mV), no particle aggregation was found (Fig. 1D).

DSC was employed to investigate the melting behavior of the lipid mixtures and MEL-NLC. Thermograms (Fig. 2A) showed an endothermic peak of 72.22 °C for the lipid mixture with MEL, and the lipid mixture without MEL had a melting point of 73.14 °C. Regarding to the formulations, the empty and the loaded NLC presented a melting temperature of 72.89 °C and 72.30 °C respectively. It can be observed that the incorporation of MEL on the bulk lipid or into the particles provoked a decrease in the melting temperature, which could be related to the accommodation of MEL into the lipid crystals, becoming more amorphous [37,38]. The melting enthalpy for the lipid mixture without MEL was 121.29 Jg⁻¹, for the lipid mixture with MEL was 119.44 Jg⁻¹, for the empty NLC was 93.76 Jg⁻¹, and for the MEL-NLC 91.91 Jg⁻¹. It was observed that the samples with a higher crystalline structure possessed the higher values, while the most amorphous sample was MEL-NLC with the lower melting enthalpy [38]. MEL melting transition was characterized by an endothermic peak at 118.52 °C ($\Delta H = 134.70$ Jg⁻¹) followed by decomposition.

FTIR spectroscopy was employed to examine the interactions between the drug, surfactant, and lipid matrix (Fig. 2B). MEL characteristic peaks were located at 3303 cm⁻¹ (N-H), 1629 cm⁻¹ (C=O), 1555 cm⁻¹ (C-O), and 1212 cm⁻¹ (C-N). The NLC (empty and loaded) spectra displayed a prominent peak at 1100 cm⁻¹, which corresponds to the surfactant [39]. Discrete MEL peaks were observed in the MEL-NLC spectrum at 1000–1200 cm⁻¹. No evidence of strong bonds between MEL, the lipid phase, and the surfactant were detected.

XRD profiles demonstrated the physical state of MEL encapsulated in NLC (Fig. 2C). MEL and the lipid bulk exhibit a crystalline structure as evidenced by prominent and sharp peaks. Certain characteristic MEL peaks (19.13, 19.94, and 24.27°) exhibited a minor intensity in the MEL-NLC profile, suggesting that the drug exists in a dissolved state within the NLC (molecular dispersion). The crystallinity of the other formulation components was also examined. The physical mixture of the lipids and the physical mixture containing MEL revealed two pronounced peaks at 21.17° (2θ) i.e., $d = 0.42$ nm and 23.09° (2θ) i.e., $d = 0.46$ nm. These peaks indicated the second stable form of triacylglycerols, the β' phase. MEL-NLC had a highly intense peak at 19.36° (2θ) i.e., $d = 0.46$ nm and 21.23° (2θ) i.e., $d = 0.42$ nm, followed by another peak at 23.27° (2θ) i.e., $d = 0.38$ nm, indicating suitable stability of the formulation [37,40,41]. In contrast, two of these peaks, at 19.36° and 23.22°, were observed in the empty NLC with lower intensity.

Table 1
Effect of cationic lipid on the physicochemical parameters.

DDAB (%)	Z _{av} ± SD (nm)	PI ± SD	ZP ± SD (mV)
0.010	293.7 ± 4.2	0.199 ± 0.032	-3.4 ± 0.2
0.025	200.4 ± 2.4	0.219 ± 0.003	0.9 ± 0.3
0.050	179.5 ± 2.6	0.193 ± 0.004	10.2 ± 0.2
0.060	172.1 ± 1.5	0.231 ± 0.013	13.1 ± 0.6
0.070	164.2 ± 0.6	0.212 ± 0.013	19.2 ± 0.7
0.080	135.7 ± 0.8	0.364 ± 0.011	20.6 ± 0.4
0.090	130.4 ± 0.2	0.480 ± 0.009	24.1 ± 0.6

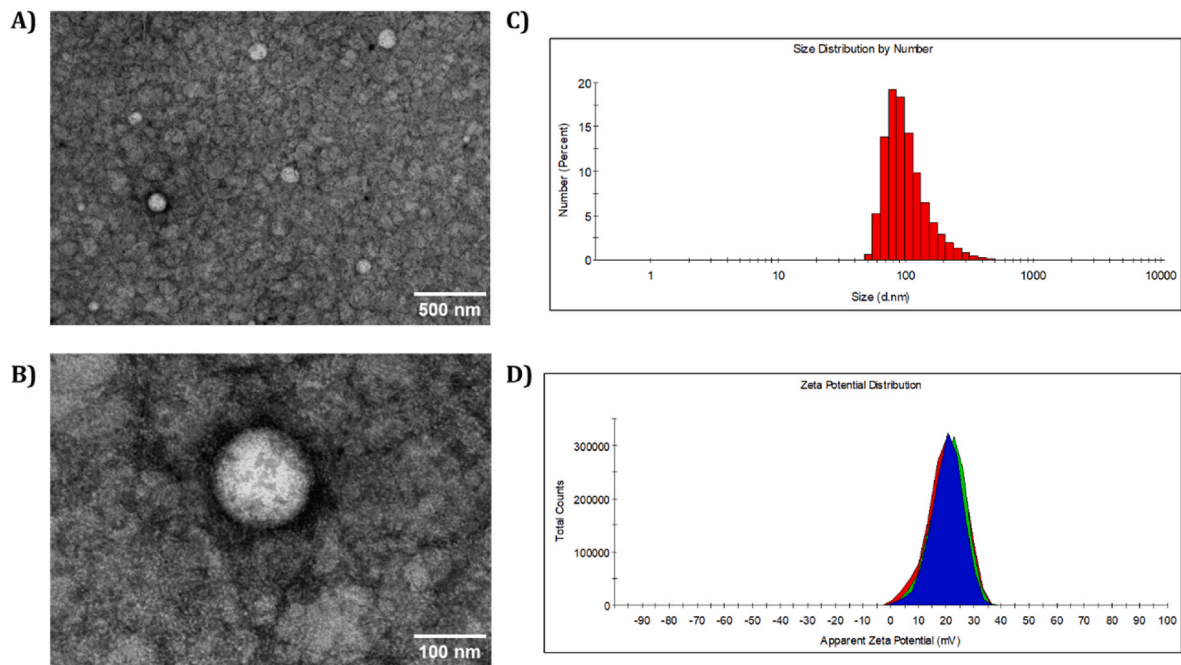


Fig. 1. Physicochemical and morphological characterization. (A) TEM images with scale bar 500 nm; (B) TEM images with scale bar 100 nm; (C) Histogram of average size distribution measured by dynamic light scattering; (D) Zeta potential plot measured by laser-Doppler electrophoresis.

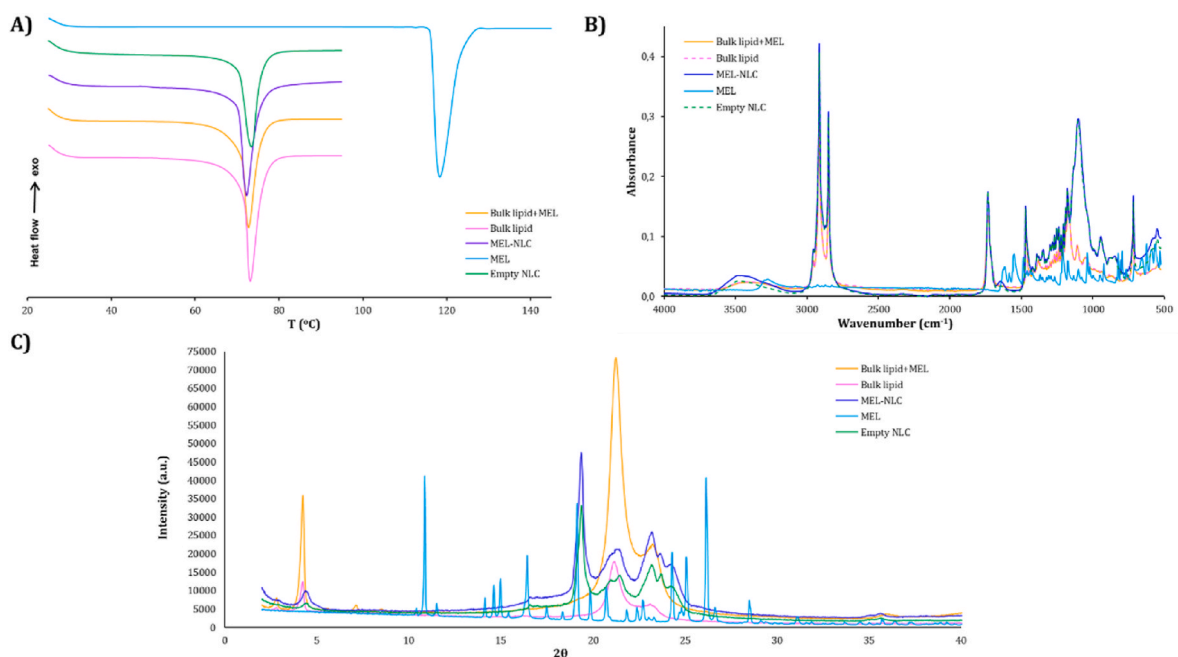


Fig. 2. Interaction studies of MEL-NLC and their components. (A) DSC curves; (B) FTIR analysis; (C) XRD patterns.

3.3. Stability studies

Stability studies were conducted using BS profiles of each sample at different temperatures (Fig. 3). BS profiles provide insights into the destabilization mechanisms, including sedimentation, aggregation, and agglomeration. In this context, BS profiles of MEL-NLC were investigated at 4, 25, and 37 °C. MEL-NLC formulation demonstrated stability at 4 °C for a period of 5 months, whilst at 25 °C, stability lasted for 15 days (BS differences >10 %). Physicochemical parameters remained consistent at 4 °C throughout the investigation (Table 2). The optimal storage temperature of 4 °C was consequently chosen.

3.4. Biopharmaceutical behaviour

The *in vitro* release profile of MEL from the NLC exhibits a slow and sustained release kinetics, indicative of a prolonged drug delivery formulation (Fig. 4). The best fit model for free MEL was exponential plateau ($r^2 = 0.9873$) and for MEL-NLC was the two-phase association ($r^2 = 0.9845$). The MEL solution achieved the 100 % before the first 7 h following a zero-order kinetic, while MEL-NLC reached the plateau after the first 24 h approximately a 77 % adhering to a first-order kinetic. The liberation of MEL from MEL-NLC showed a first fast release, with a higher kinetic constant (K_d) and a shorter half-life time ($t_{1/2}$, the time

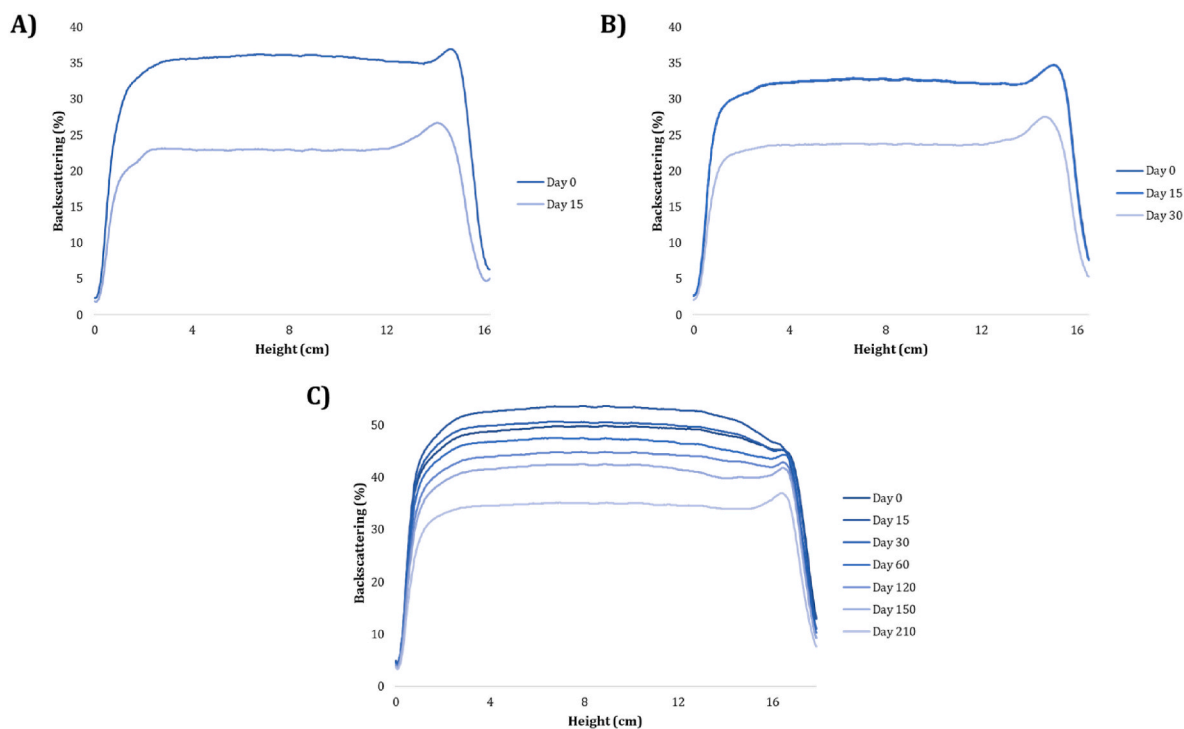


Fig. 3. Backscattering profiles of MEL-NLC stored at (A) 37 °C, (B) 25 °C, and (C) 4 °C.

Table 2
Physicochemical parameters of MEL-NLC stored at different temperatures.

Temperature (°C)	Day	Z _{av} ± SD (nm)	PI ± SD	ZP ± SD (mV)	EE ± SD (%)
37	0	168.9 ± 2.4	0.216 ± 0.007	19.1 ± 0.5	79.8 ± 0.2
	15	193.8 ± 0.3	0.232 ± 0.007	14.4 ± 0.3	75.1 ± 0.5
25	15	170.1 ± 0.7	0.200 ± 0.004	18.0 ± 0.1	78.4 ± 0.1
	30	230.4 ± 3.1	0.224 ± 0.035	11.7 ± 0.5	76.1 ± 0.2
4	15	162.0 ± 1.2	0.218 ± 0.012	20.3 ± 0.9	77.9 ± 0.6
	30	163.1 ± 0.8	0.221 ± 0.007	20.5 ± 0.4	78.4 ± 0.1
	60	167.8 ± 1.5	0.213 ± 0.015	21.2 ± 0.9	76.8 ± 0.8
	120	166.2 ± 1.4	0.218 ± 0.021	19.2 ± 0.4	78.9 ± 0.3
	150	167.1 ± 0.8	0.234 ± 0.007	20.5 ± 0.4	77.1 ± 0.4
	210	179.9 ± 0.1	0.268 ± 0.016	18.7 ± 0.4	77.6 ± 0.1

required for the initial concentration to decrease to one-half). In contrast, the slow and sustained release phase of MEL-NLC had the slowest K_d and the highest t_{1/2}.

3.5. Ocular tolerance

Ocular tolerance was assayed *in vitro* and *in vivo* (Fig. 5) examining free MEL and MEL-NLC. Previous to this assay, DDAB ocular tolerance was assessed by HET-CAM at the maximum concentration reported as safe in other studies (0.5 %), confirming that it was non-irritant. Afterwards, the developed NLC resulted non-irritant neither *in vitro* nor *in vivo*, while the free MEL resulted moderately irritating *in vitro* and non-

irritant *in vivo*. Although the HET-CAM test is useful for assessing eye irritation from water-soluble and surfactant-based substances, and that it is useful to identify non-irritant compounds, such as MEL-NLC, occasionally it could show a poor correlation with the *in vivo* assays, as it is observed in the case of free MEL, which resulted non-irritant *in vivo* [42].

3.6. Cellular experiments

3.6.1. Cell viability

The cytotoxicity of free MEL and MEL-NLC formulations was determined on HCE-2 cells to assess their compatibility with corneal cells following topical application (Fig. 6A). Samples were incubated for 5, 15, and 30 min to simulate the *in vivo* contact between the formulation and the human cornea. Cell viability was assessed using ISO 10993-5 guidelines, where viability above 80 % indicates non-cytotoxicity, 60–80 % weak cytotoxicity, 40–60 % moderate cytotoxicity, and below 40 % indicates strong cytotoxicity. Results demonstrated that free MEL exhibited minimal cytotoxic effects on HCE-2 cells, with viability remaining above 80 % for all tested concentrations and incubation times. Otherwise, the most concentrated dilutions of MEL-NLC (0.1 mg/mL) resulted moderately toxic at all the incubation times, which could be related to the high electrostatic interaction between the negatively charged surface with the cationic NLC [43]. All the other concentrations resulted weakly toxic for the corneal cells.

The cytotoxic effect exerted on the tumoral cells is shown in Fig. 6B. It can be observed that in most of the studied concentrations, MEL-NLC showed a significantly higher antitumoral effect than the free MEL, probably, because of the slow release of MEL and the increased cell penetration of MEL-NLC, leading to a higher cytotoxic effect. In the diluted concentrations, free MEL did not show toxicity to the UM cells after 24 h.

3.6.2. Cellular uptake

The cellular uptake of MEL-NLC was investigated in the HCE-2 cell line. Following various incubation times, the fluorescent NLC were visualized by fluorescence microscopy. The nucleus was stained with DAPI and the cell membrane with Alexa Fluor™ 488-WGA. The merged

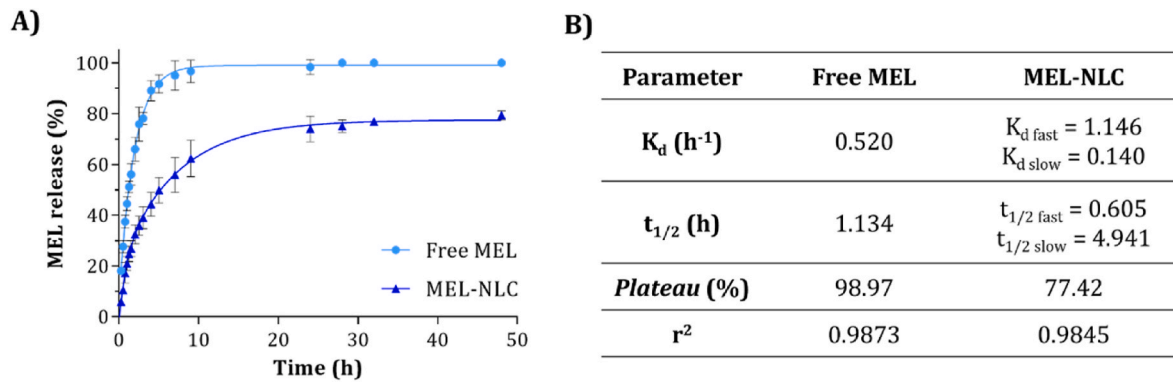


Fig. 4. *In vitro* release profile of free MEL against MEL-NLC performed by triplicate. (A) Release profile graphical representation of MEL-NLC vs free MEL carried out for 48 h. Results were expressed on drug accumulative release percentage (%) vs sampling time point (h), (B) adjustment to a two-phase association (MEL-NLC) and exponential plateau model (free MEL).

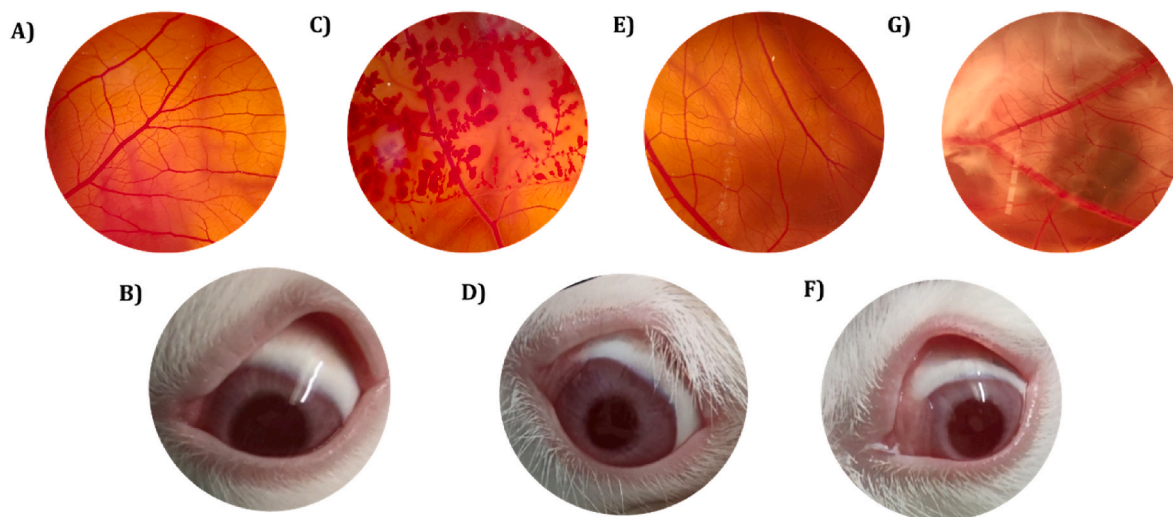


Fig. 5. *In vitro* and *in vivo* irritation assay. (A–B) Negative control, NaCl 0.9% and untreated contralateral eye respectively, (C) Positive control, NaOH 0.1 M, (D–E) Free MEL and (F–G) MEL-NLC.

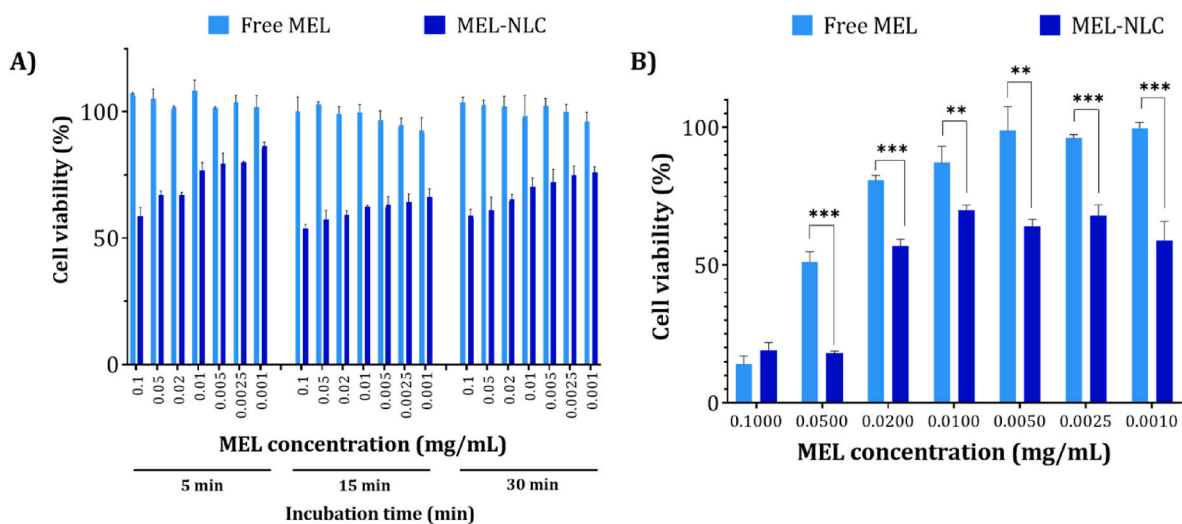


Fig. 6. Cell viability assays on HCE-2 and UM-92-1 cells, experiments were assessed in triplicate, and the experiments were repeated up to 5 times. The results were expressed as the percentage of viable cells compared to untreated control cells. (A) Effect of free MEL and MEL-NLC on the viability of HCE-2 cells at 5, 15 and 30 min, (B) Cytotoxic effects of free MEL and MEL-NLC on UM-92-1 cells at 24 h.

images (Fig. 7) revealed the presence of MEL-NLC inside the cells, mainly in the cytoplasm, indicating that the particles successfully penetrated the corneal cells without disrupting their morphology, such as vacuolization caused by benzalkonium chloride [44]. Additionally, the fluorescence signal intensified with increasing incubation time. Analysis using Interactive 3D Surface Plot in ImageJ confirmed this observation and demonstrated that cells incubated with MEL-NLC for 30 min exhibited higher fluorescence intensity compared to those incubated for 5 or 15 min. No fluorescence was detected in control cells.

3.7. In vivo experiments

3.7.1. Anti-inflammatory efficacy

To evaluate the anti-inflammatory efficacy of MEL-NLC *in vivo*, the capacity to prevent and treat ocular inflammation was investigated.

The efficacy of NLC in preventing inflammation was examined. Treatments were administered 30 min before exposure to SA, and the severity of inflammation was assessed. Fig. 8A demonstrates a significant reduction in inflammation after 30 min exposure to SA. Free MEL exhibited a slower reduction in corneal swelling compared to MEL-NLC.

This difference can be attributed to tear clearance, which rapidly removes free MEL from the ocular surface. In contrast, MEL-NLC exhibit enhanced adhesion to the cornea, enabling them to remain in the ocular environment for a longer timepoints, thereby providing sustained anti-inflammatory effects. Furthermore, MEL-NLC demonstrated significant differences compared to the positive control and free MEL over time ($p < 0.001$).

The efficacy of NLC as a treatment for inflammation was further evaluated *in vivo*. Treatments were administered 30 min after SA exposure, and the severity of inflammation was assessed at various time points. Fig. 8B shows a significant reduction in inflammation within 120 min following MEL-NLC administration. This slower but effective anti-inflammatory response can be attributed to the controlled release of NLC. Otherwise, free MEL showed a faster onset of anti-inflammatory activity compared to MEL-NLC. This difference can be attributed to the controlled release of MEL from NLC, which prolongs its therapeutic effect but delays its initial delivery.

3.7.2. In vivo biodistribution

To visualize the distribution of MEL-NLC after topical ophthalmic

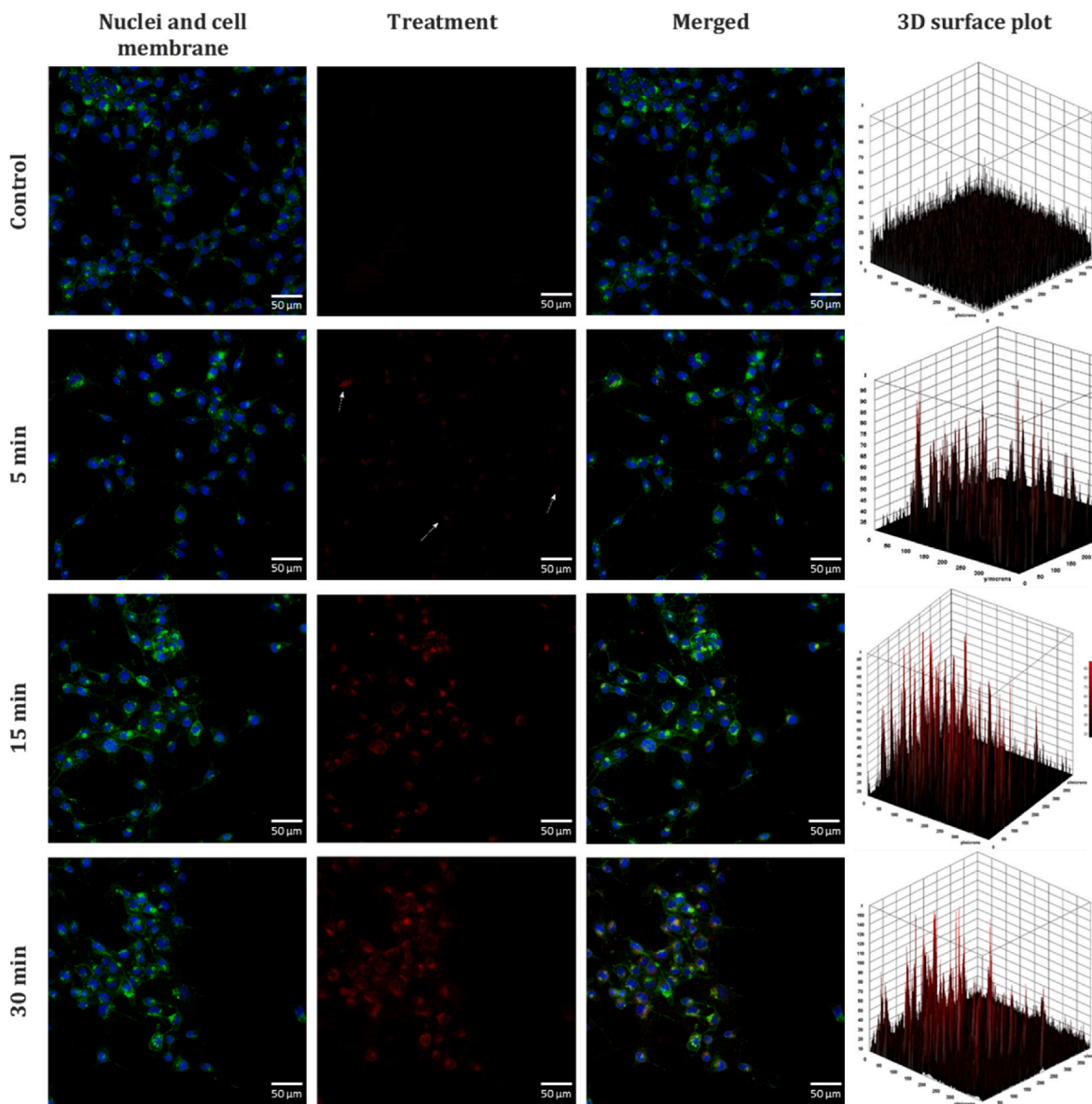


Fig. 7. Cellular uptake of MEL-NLC in HCE-2 at different incubation time (5, 15, or 30 min). White arrows highlight the samples localization, scale bar 50 μm .

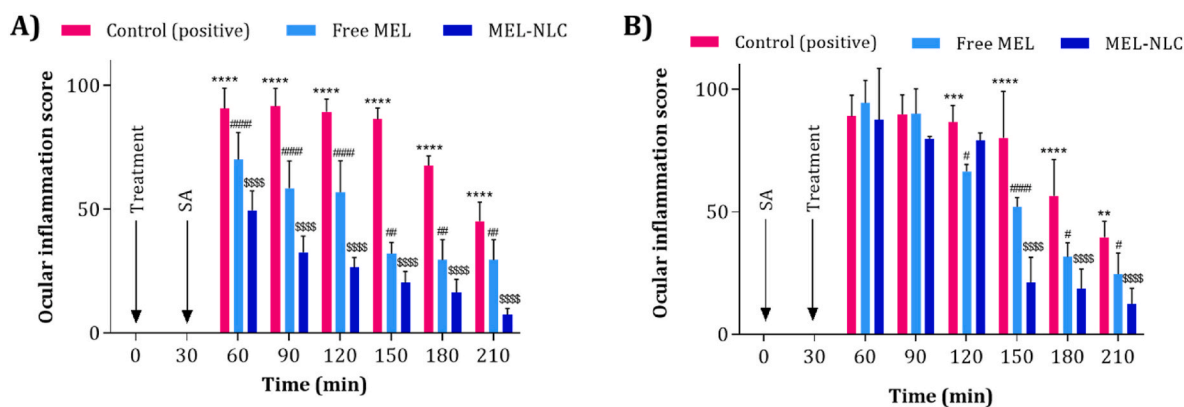


Fig. 8. Comparison of ocular anti-inflammatory efficacy of free MEL and MEL-NLC. (A) Inflammation prevention, (B) inflammation treatment. Values are expressed as mean \pm SD; ** $p < 0.01$, *** $p < 0.005$, and **** $p < 0.001$ significantly lower effect of free MEL than the inflammatory effect induced by SA; \$\$\$ $p < 0.001$ significantly lower effect of MEL-NLC than the inflammatory effect induced by SA; # $p < 0.05$, ## $p < 0.01$ and ### $p < 0.001$ significantly lower effect of MEL-NLC than the free MEL.

administration, NR, a lipophilic probe, was encapsulated into NLC, resulting in the formation of MEL-NLC-NR. Topical administration of both MEL-NLC-NR and free NR solution was performed on New Zealand albino rabbits to investigate the *in vivo* biodistribution. After 3 h, animals were sacrificed, and their eyes were collected and subsequently sliced. Whole eye images were analysed, and their fluorescence intensity was quantified in order to establish the biolocalization of the formulation. Fluorescence microscopy analysis revealed that MEL-NLC-NR appeared to accumulate in the posterior segment of the eye, specifically in the retina. Fig. 9A shows statistical differences between the 3 studied groups. Control eyes showed some retinal autofluorescence, mainly caused by the photoreceptors and retinal pigment epithelium [45]. Moreover, no statistically significant differences in the mean fluorescent intensity (MFI) between NR and the control were found indicating that no NR was able to achieve posterior segment tissues after 3 h. Moreover, MEL-NLC-NR showed significant differences between both control and NR, which indicates that the formulation achieved the inner tissues of the eye, specifically, the retina (Fig. 9B).

4. Discussion

UM is a rare type of ocular cancer, in which approximately a 50 % of patients develop metastases [5]. In the present study, a formulation loading MEL into a cationic rosehip-based NLC has been developed. Based on a prior formulation developed, the incorporation of a cationic surfactant shifted surface charge towards a positive, probably enhancing

MEL-NLC adhesion to the ocular mucosa and promoting their bioavailability upon topical administration. This is particularly advantageous due to the negatively charged mucus layer that coats the corneal surface. In this area, cationic surfactants facilitate electrostatic interactions between the positively charged nanoparticle surface and the anionic ocular mucosa, leading to a prolonged drug residence time. Among cationic surfactants, DDAB demonstrated minimal ocular toxicity and reduced irritation potential compared to other cationic surfactants [46,47].

To optimize the concentration of DDAB in the formulation, incremental amounts were incorporated. The preferable amount of DDAB should achieve suitable physicochemical parameters for ocular delivery, such as a small size below 200 nm, PI under 0.3 and a ZP around +20 mV [16]. Increasing amounts of DDAB led to smaller particle sizes, which could be related to the reduction of the surface tension [48]. PI was maintained around 0.2 until 0.08 % DDAB, whereas at higher concentrations increased over 0.3. ZP varied from negative to positive surface charge, in which the concentrations up to 0.07 % DDAB produced a ZP around +20 mV. Based on these parameters, the optimal DDAB amount was 0.07 % since it accomplished suitable physicochemical parameters suitable for ocular administration.

Using this formulation, interaction studies demonstrated the successful incorporation of MEL into NLC [49]. DSC analysis revealed that MEL-NLC exhibited the lowest melting point, indicating a highly amorphous state, probably due to the incorporation of the drug inside the amorphous lipid structure. This could prevent expulsion of the drug from the nanoparticles during storage [50]. In comparison to the

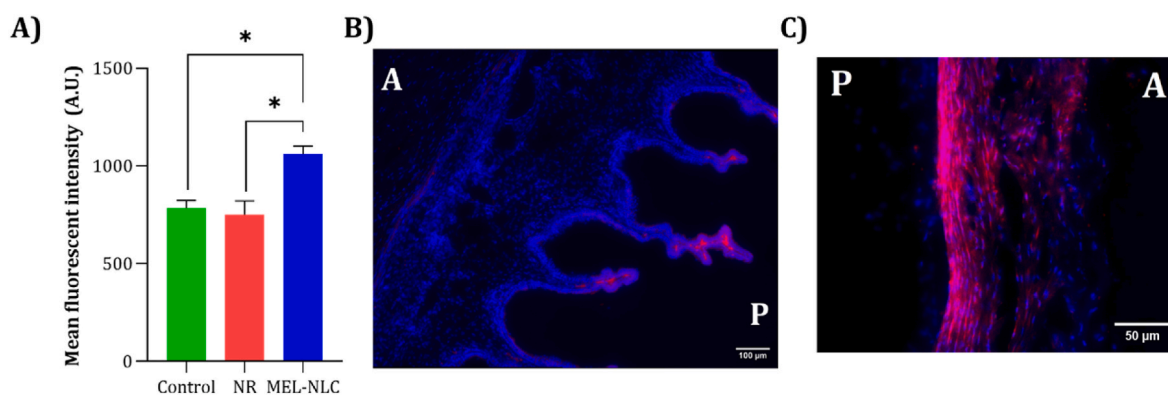


Fig. 9. Biodistribution studies performed in New Zealand rabbits. (A) Comparison of mean fluorescent intensity on the posterior eye part of a control, NR solution and MEL-NLC labeled to NR. (B) Fluorescent image of a rabbit ciliary processes treated with MEL-NLC-NR (in red) showed with a scale bar of 100 μ m. (C) Fluorescent image of a rabbit sclera treated with MEL-NLC-NR (in red) showed with a scale bar of 50 μ m. (For interpretation of the references to colour in this figure legend, the reader is referred to the Web version of this article.)

negatively charged NLC, the cationic formulation presented higher melting enthalpies for all the mixtures (bulk lipid, empty NLC or loaded NLC). This fact indicates that the positive formulation shifts towards a more crystalline structure, since higher energy was necessary to achieve the melting point, thus leading to a reduced stability in comparison to the prior formulation [17,40]. Further analysis employing FTIR spectroscopy indicated the absence of covalent bonds between MEL and the lipid matrix, suggesting that their interaction was primarily mediated by non-covalent forces, such as hydrogen bonds and hydrophobic interactions [51]. Additionally, XRD studies showed characteristic peaks of the stable forms of triacylglycerols, known as the β and β' forms [37,40,41]. However, the formulation showed a reduced stability in comparison to the negatively charged NLC from previous studies, which was 16 months at 4 °C, probably due to the increase in the crystallinity degree caused by this DDAB addition [17]. Moreover, the samples at higher temperatures (25 and 37 °C) showed a short stability, which could be related to their Brownian motion, increasing their collision frequency, facilitating their destabilization [52]. Furthermore, MEL-NLC demonstrated sustained *in vitro* release, in contrast to MEL solution, which exhibited a rapid release profile. Release studies revealed that MEL solution achieved its *plateau* rapidly, reaching approximately 100 % drug release within the first few hours. In contrast, MEL-NLC required approximately 24 h to reach its *plateau*, releasing approximately 78 % of the drug into the receptor medium. In comparison to previous studies [17], in which the negatively charged formulation was prepared, the initial burst phase was much faster in the positively formula, with a higher K_d and a lower $t_{1/2}$ (K_d of 1.15 vs 0.32 h⁻¹, and $t_{1/2}$ of 0.60 vs 2.16 h from positive and negative formulation respectively). Furthermore, the prolonged release phase was faster in the positive formula (K_d of 0.14 vs 0.06 h⁻¹, and $t_{1/2}$ of 4.94 vs 11.52 h from positive and negative formulation respectively). Other studies reported differences between the release of different drugs from lipid nanoparticles regarding their composition. Specifically, Zoubari et al. [53] found that the addition of a different lipid into the formulation resulted in a faster drug release due to the less organized lipid matrix, making softer particles. Regarding to the kinetic order, the free drug adhered to a zero-order kinetic, in which the drug is released at a constant rate [54]. Otherwise, MEL-NLC adhered to a first-order kinetic, in which the amount of drug released is proportional to the amount of remaining drug in the matrix. Thus, the amount of active released tends to decrease in function of time, creating a sustained and slow release [55]. This kinetics were also observed by Shafiee et al. [56] in their polymeric film incorporating metronidazole, in which the drug was released slowly during a week, reaching the plateau after 4 days. Our results among to the stability and interaction studies could mean that the addition of the cationic surfactant DDAB could result in a more ordered lipid structure, which decreased its stability, and increased MEL release, which could be favourable in order to achieve higher amounts in a faster manner into the inner tissues of the eye.

To assess ocular safety of the formulated drug, *in vitro* and *in vivo* evaluations were performed. The *in vitro* HET-CAM test revealed that MEL-NLC exhibited no irritation upon direct application to the chorio-lantoic membrane. Additionally, the HET-CAM TBS assay, a quantitative method based on trypan blue uptake to assess cell viability, confirmed the lack of significant cellular damage induced by MEL-NLC. Free MEL resulted moderately irritating *in vitro*, fact that other studies have also reported [57]. However, this data could be related to the use of organic solvents or surfactants that are necessary to ensure MEL solubilization [58]. Subsequently, an *in vivo* ocular Draize test was conducted to further evaluate the formulations safety. The results demonstrated that free MEL and MEL-NLC did not cause any ocular irritation or redness in animal eyes, indicating their safety for ocular administration.

Moreover, *in vitro* studies confirmed that free MEL was non-toxic in corneal cells in all the studied concentrations. These findings agreed with the role of MEL into the eye under physiological conditions, in which mainly MEL is a regulator of physiological circadian rhythm

processes [59]. Regarding to the formulation, it was found that with 5 min incubation time, the concentrations up to 0.01 mg/mL MEL-NLC resulted non-toxic. These results were significant due to the real residence time of formulations into the ocular surface, which usually is very reduced due to the nasolacrimal clearance [60,61]. Otherwise, when incubation time was increased, the formulation showed a weak toxicity in all the tested concentrations. This effect could be attributed to several factors, including the positive charge of the lipid NLC, which promotes electrostatic interaction with the negatively charged cell surfaces. This interaction could lead to an increase in oxidative stress and reactive oxygen species (ROS) [62]. Additionally, NLC exhibit high affinity for cells, facilitating their interaction [63]. These facts were observed during the internalization study, in which from the first 5 min until 30 min incubation time, MEL-NLC were internalized into the cells, increasing the fluorescence signal at longer timepoints. Furthermore, in despite cell viability assays resulted in a weak toxicity, the morphology of the cells did not change or showed vacuolization, which is related to toxic substances in corneal cells [44].

In order to assess the potential activity of the nanoformulation against UM, cytotoxicity was assessed in UM cells. For free MEL, the most concentrated dilutions caused cytotoxic effects. Previous studies reported that MEL in UM cells was active in a range of 0.1–10 nM [64]. However, in our studies, the concentrations able to achieve cytotoxic effects were higher which may be due to the increased cell density used (3×10^3 vs 1×10^4 cells/well respectively). It has been reported that when higher cell density is used, it could result in lower cytotoxicity [65]. Regarding MEL-NLC, the two most concentrated dilutions resulted in high cytotoxicity (<20 % cell viability), while the other tested dilutions were moderately cytotoxic (40–60 % cell viability). The higher cytotoxicity could be related to the increased release of MEL inside the tumoral cells, improving its bioavailability and therapeutic efficacy. Furthermore, other investigations have reported that UM cells express transmembrane receptors for MEL, and its membrane receptor agonists inhibited the growth of UM cells even at low concentrations [7]. These findings could also contribute to the highest activity of MEL-NLC, as in addition to the high penetration of NLC into cells, non-encapsulated MEL or the initial burst release of MEL could also be effective by reaching the membrane receptors of the UM cells.

Inflammation is a hallmark of cancer development and progression, involving a complex interplay between immune cells, stromal cells, and tumor microenvironment [66]. The cells contributing to cancer-associated inflammation are relatively genetically stable, exhibiting lower rates of drug resistance compared to cancer cells themselves. Therefore, targeting inflammation represents a promising strategy for both cancer prevention and therapy [67]. Despite decades of research, the precise role of inflammation in UM progression remains poorly understood. UM tumors exhibit an inflammatory phenotype characterized by abundance of immune mediators and proinflammatory cytokines in their surrounding microenvironment [68]. For this reason, the potential anti-inflammatory activity of MEL-NLC was performed. In the treatment and prevention assays, it was observed that MEL had a great anti-inflammatory action. It is well known that MEL possesses protective properties against various ocular disorders, including photokeratitis, cataract, retinopathy of prematurity, and ischemic/reperfusion injury [69]. Additionally, MEL has been shown to mitigate retinal damage associated with glaucoma and diabetes [70]. In this area, Meng et al. [71] explored the anti-inflammatory activity of MEL after a corneal alkali injury in mice model. They reported that the infiltration of inflammatory cells and pro-inflammatory cytokines, such as TNF- α , IL-1 β and IL-6 were reduced after MEL treatment. In another study, ocular uveitis was induced with an injection of lipopolysaccharide (LPS) and posteriorly treated with MEL. It was observed that the leakage of cells and proteins decreased. Also, MEL treatment protected the retinal structure and decreased NOS activity, lipid peroxidation and TNF- α [70]. Otherwise, MEL-NLC showed greater anti-inflammatory activity, probably because of the increased delivery of MEL into the ocular

tissues, and its prolonged release.

Finally, *in vivo* biodistribution confirmed the ability of MEL-NLC to reach the inner tissues of the eye. Mainly, the formulation showed high affinity for the retina, and also it was retained in the ciliary processes. Its relatively high penetration could be related to the small size of the nanocarrier, its lipid matrix nature, and its improved mucoadhesion properties because of the cationic surface charge. Other studies confirmed that NLC were able to increase drug penetration rate, increasing drug levels into ocular tissues [72]. Moreover, numerous studies have highlighted the enhanced interaction of cationic nanoparticles with the ocular surface [73–76]. For instance, a study investigated the mucoadhesive properties of cationic nanoparticles loaded with an antifungal drug. The results revealed a strong interaction between the negatively charged mucins of the ocular surface and the nanoparticles, demonstrating their potential for targeted drug delivery to ocular tissues [73]. These findings are relevant due to the location of UM tumors, which are the ciliary body and choroids [4]. As MEL-NLC had an increased accumulation on the inner tissues of the eye, the formulation could be able to target these tumors and release MEL, increasing its therapeutic activity.

5. Conclusions

This study introduces a novel formulation of cationic lipid nanoparticles capable of encapsulating MEL for topical ophthalmic administration. MEL-NLC exhibit suitable physicochemical characteristics, including particle size below 200 nm, monomodal size distribution, spherical shape, and suitable stability. Encapsulation of MEL within NLC significantly enhanced its therapeutic efficacy, both *in vitro* and *in vivo*, demonstrating potent preventive and therapeutic anti-inflammatory activities. Furthermore, *in vitro* studies demonstrated selective cytotoxicity in uveal melanoma cells and *in vivo* biodistribution studies using fluorescent-labeled NLC suggested their ability to penetrate to the posterior ocular segment, potentially targeting uveal melanoma.

CRedit authorship contribution statement

Lorena Bonilla-Vidal: Writing – original draft, Methodology, Investigation. **Marta Espina:** Writing – review & editing, Supervision. **María Luisa García:** Methodology, Investigation, Funding acquisition. **Cinzia Cimino:** Writing – review & editing, Methodology. **Claudia Carbone:** Writing – review & editing, Methodology. **Laura Baldomà:** Methodology, Investigation, Funding acquisition. **Josefa Badia:** Methodology, Investigation, Funding acquisition. **Anna Gliszczynska:** Writing – review & editing, Supervision. **Eliana B. Souto:** Methodology, Investigation, Funding acquisition. **Elena Sánchez-López:** Writing – review & editing, Supervision, Methodology, Investigation, Funding acquisition.

Declaration of competing interest

The authors declare that they have no known competing financial interests or personal relationships that could have appeared to influence the work reported in this paper.

Data availability

No data was used for the research described in the article.

Acknowledgment

This research was supported by the Ministerio de Ciencia, Innovación y Universidades (MICIU) under the reference PID2021-122187NB-C32. E.S.-L. acknowledges the support of Grants for the Requalification of the Spanish University System.

References

- [1] E.S. Rantala, M.M. Hernberg, S. Piperno-Neumann, H.E. Grossniklaus, T.T. Kivela, Metastatic uveal melanoma: the final frontier, *Prog. Retin. Eye Res.* 90 (2022) 101041.
- [2] K.N. Smit, M.J. Jager, A. de Klein, E. Kiliç, Uveal melanoma: towards a molecular understanding, *Prog. Retin. Eye Res.* 75 (2020) 100800.
- [3] J. Yang, D.K. Manson, B.P. Marr, R.D. Carvajal, Treatment of uveal melanoma: where are we now? *Ther. Adv. Med. Oncol.* 10 (2018).
- [4] M.J. Jager, C.L. Shields, C.M. Cebulla, M.H. Abdel-Rahman, H.E. Grossniklaus, M. H. Stern, et al., Uveal melanoma, *Nat. Rev. Dis. Prim.* 6 (1) (2020) 24.
- [5] R.D. Carvajal, J.J. Sacco, M.J. Jager, D.J. Eschelmann, R. Olofsson Bagge, J. W. Harbour, et al., Advances in the clinical management of uveal melanoma, *Nat. Rev. Clin. Oncol.* 20 (2) (2023) 99–115.
- [6] F. Moradkhani, M. Moloudizargari, M. Fallah, N. Asghari, H. Heidari Khoei, M. H. Asghari, Immunoregulatory role of melatonin in cancer, *J. Cell. Physiol.* 235 (2) (2020) 745–757.
- [7] A. Hagström, Omar R. Kal, P.A. Williams, G. Stålhammar, The rationale for treating uveal melanoma with adjuvant melatonin: a review of the literature, *BMC Cancer* 22 (1) (2022) 1–17.
- [8] Omar R. Kal, A. Hagström, G. Stålhammar, Adjuvant melatonin for uveal melanoma (AMUM): protocol for a randomized open-label phase III study, *Trials* 24 (1) (2023) 1–14.
- [9] V. Lopes, J. Assis, T. Ribeiro, G. de Castro, M. Pacheco, L. Borges, et al., Melatonin loaded lecithin-chitosan nanoparticles improved the wound healing in diabetic rats, *Int. J. Biol. Macromol.* 162 (2020) 1465–1475.
- [10] L. Xie, W. Yue, K. Ibrahim, J. Shen, A long-acting curcumin nanoparticle/in situ hydrogel composite for the treatment of uveal melanoma, *Pharmaceutics* 13 (9) (2021) 1335.
- [11] K. Bilmin, K.J. Synoradzki, A.M. Czarna, M.J. Spalek, T. Kujawska, M. Solnik, et al., New perspectives for eye-sparing treatment strategies in primary uveal melanoma, *Cancers* 14 (1) (2022) 134.
- [12] A. Narvekar, C. Rich, A. Savinainen, I.K. Kim, Nanoparticles for the treatment of uveal melanoma, *Uveal Melanoma Biol. Manag.* (2021) 135–149.
- [13] H. Sabit, M. Abdel-Hakeem, T. Shoala, S. Abdel-Ghany, M.M. Abdel-Latif, J. Almulhim, et al., Nanocarriers: a reliable tool for the delivery of anticancer drugs, *Pharmaceutics* 14 (8) (2022) 1566.
- [14] S. Nasirizadeh, B. Malaekheh-Nikouei, Solid lipid nanoparticles and nanostructured lipid carriers in oral cancer drug delivery, *J. Drug Deliv. Sci. Technol.* 55 (2020) 101458.
- [15] L. Bayón-Cordero, I. Alkorta, L. Arana, Application of Solid Lipid Nanoparticles to improve the efficiency of anticancer drugs, *Nanomaterials* 9 (3) (2019) 474.
- [16] L. Bonilla, M. Espina, P. Severino, A. Cano, M. Etxcheto, A. Camins, et al., Lipid nanoparticles for the posterior eye segment, *Pharmaceutics* 14 (1) (2022) 90.
- [17] L. Bonilla-Vidal, M. Switalska, M. Espina, J. Wietrzyk, M.L. García, E.B. Souto, A. Gliszczynska, E. Sánchez-López, Antitumoral melatonin-loaded nanostructured lipid carriers, *Nanomedicine* (2024) 1–16.
- [18] J.F. Fanguero, A.C. Calpena, B. Clares, T. Andreani, M.A. Egea, F.J. Veiga, et al., Biopharmaceutical evaluation of epigallocatechin gallate-loaded cationic lipid nanoparticles (EGCG-LNs): *in vivo*, *in vitro* and *ex vivo* studies, *Int. J. Pharm.* 502 (1–2) (2016) 161–169.
- [19] A.M. Silva, C. Martins-Gomes, J.F. Fanguero, T. Andreani, E.B. Souto, Comparison of antiproliferative effect of epigallocatechin gallate when loaded into cationic solid lipid nanoparticles against different cell lines, *Pharmaceut. Dev. Technol.* 24 (10) (2019) 1243–1249.
- [20] L. Bonilla-Vidal, M. Espina, M.L. García, L. Baldomà, J. Badia, J.A. González, et al., Novel nanostructured lipid carriers loading Apigenin for anterior segment ocular pathologies, *Int. J. Pharm.* 658 (2024) 124222.
- [21] J. Hou, M. Karin, B. Sun, Targeting cancer-promoting inflammation — have anti-inflammatory therapies come of age? *Nat. Rev. Clin. Oncol.* 18 (5) (2021) 261–279.
- [22] G. Esteruelas, L. Halbaut, V. García-Torra, M. Espina, A. Cano, M. Etxcheto, et al., Development and optimization of Riluzole-loaded biodegradable nanoparticles incorporated in a mucoadhesive *in situ* gel for the posterior eye segment, *Int. J. Pharm.* 612 (2022) 121379.
- [23] E. Sánchez-López, G. Esteruelas, A. Ortiz, M. Espina, J. Prat, M. Muñoz, et al., Dexibuprofen biodegradable nanoparticles: one step closer towards a better ocular interaction study, *Nanomaterials* 10 (4) (2020).
- [24] X. Llorente, G. Esteruelas, L. Bonilla, M.G. Agudelo, I. Filgaira, D. Lopez-Ramajo, et al., Riluzole-loaded nanostructured lipid carriers for hyperproliferative skin diseases, *Int. J. Mol. Sci.* 24 (9) (2023) 8053.
- [25] E. Sánchez-López, M. Etxcheto, M.A. Egea, M. Espina, A. Cano, A.C. Calpena, et al., Memantine loaded PLGA PEGylated nanoparticles for Alzheimer's disease: *in vitro* and *in vivo* characterization, *J. Nanobiotechnol.* 16 (1) (2018) 1–16.
- [26] F. Elmsmari, J.A. González Sánchez, F. Duran-Sindreu, R. Belkadi, M. Espina, M. L. García, et al., Calcium hydroxide-loaded PLGA biodegradable nanoparticles as an intracanal medicament, *Int. Endod. J.* 54 (11) (2021) 2086–2098.
- [27] R. Galindo, E. Sánchez-López, M.J. Gómara, M. Espina, M. Etxcheto, A. Cano, et al., Development of peptide targeted PLGA-PEGylated nanoparticles loading Licochalcone-A for ocular inflammation, *Pharmaceutics* 14 (2) (2022) 285.
- [28] C. Folle, A.M. Marqués, N. Díaz-Garrido, M. Espina, E. Sánchez-López, J. Badia, et al., Thymol-loaded PLGA nanoparticles: an efficient approach for acne treatment, *J. Nanobiotechnol.* 19 (1) (2021) 359.
- [29] R. Gonzalez-Pizarro, P. Carvajal-Vidal, L. Halbaut Bellowa, A.C. Calpena, M. Espina, M.L. García, *In-situ* forming gels containing fluorometholone-loaded polymeric nanoparticles for ocular inflammatory conditions, *Colloids Surf. B Biointerfaces* 175 (2019) 365–374.

- [30] A. López-Machado, N. Díaz-Garrido, A. Cano, M. Espina, J. Badia, L. Baldomà, et al., Development of lactoferrin-loaded liposomes for the management of dry eye disease and ocular inflammation, *Pharmaceutics* 13 (10) (2021) 1698.
- [31] A. Lagarto, R. Vega, I. Guerra, R. González, In vitro quantitative determination of ophthalmic irritancy by the chorioallantoic membrane test with trypan blue staining as alternative to eye irritation test, *Toxicol. Vitro* 20 (5) (2006) 699–702.
- [32] C. Cimino, E. Sánchez López, A. Bonaccorso, L. Bonilla, T. Musumeci, J. Badia, et al., In vitro and in vivo studies of ocular topically administered NLC for the treatment of uveal melanoma, *Int. J. Pharm.* 660 (2024) 124300.
- [33] Y. Olivo-Martínez, M. Bosch, J. Badia, L. Baldomà, Modulation of the intestinal barrier integrity and repair by microbiota extracellular vesicles through the differential regulation of trefoil factor 3 in LS174T goblet cells, *Nutrients* 15 (11) (2023) 2437.
- [34] E.S. López, A.L.L. Machado, L.B. Vidal, R. González-Pizarro, A.D. Silva, E.B. Souto, Lipid nanoparticles as carriers for the treatment of neurodegeneration associated with Alzheimer's disease and glaucoma: present and future challenges, *Curr. Pharmaceut. Des.* 26 (12) (2020) 1235–1250.
- [35] R. Gonzalez-Pizarro, G. Parrotta, R. Vera, E. Sánchez-López, R. Galindo, F. Kjeldsen, et al., Ocular penetration of fluorometholone-loaded PEG-PLGA nanoparticles functionalized with cell-penetrating peptides, *Nanomedicine* 14 (23) (2019) 3089–3104.
- [36] S. Sweetledge, R. Carter, R. Stout, C.E. Astete, J.P. Jung, C.M. Sabliov, Stability and ocular redistribution of topically administered PLGA nanoparticles, *Sci. Rep.* 11 (1) (2021) 1–11.
- [37] E.B. Souto, W. Mehnert, R.H. Müller, Polymorphic behaviour of Compritol 888 ATO as bulk lipid and as SLN and NLC, *J. Microencapsul.* 23 (4) (2006) 417–433.
- [38] H. Bunjes, K. Westesen, M.H.J. Koch, Crystallization tendency and polymorphic transitions in triglyceride nanoparticles, *Int. J. Pharm.* 129 (1–2) (1996) 159–173.
- [39] X. Fu, W. Kong, Y. Zhang, L. Jiang, J. Wang, J. Lei, Novel solid–solid phase change materials with biodegradable trihydroxy surfactants for thermal energy storage, *RSC Adv.* 5 (84) (2015) 68881–68889.
- [40] C. Freitas, R.H. Müller, Correlation between long-term stability of solid lipid nanoparticles (SLN) and crystallinity of the lipid phase, *Eur. J. Pharm. Biopharm.* 47 (2) (1999) 125–132.
- [41] E. Zimmermann, E.B. Souto, R.H. Müller, Physicochemical investigations on the structure of drug-free and drug-loaded solid lipid nanoparticles (SLN) by means of DSC and ¹H NMR, *Pharmazie* 60 (7) (2005) 508–513.
- [42] A.M. da Nóbrega, E.N. Alves, R. de Farias Presgrave, R.N. Costa, I.F. Delgado, Determination of eye irritation potential of low-irritant products: comparison of in vitro results with the in vivo draize rabbit test, *Braz. Arch. Biol. Technol.* 55 (3) (2012) 381–388.
- [43] M. Adabi, M. Naghibzadeh, M. Adabi, M.A. Zarrinfard, S.S. Esnaashari, A. M. Seifalian, et al., Biocompatibility and nanostructured materials: applications in nanomedicine, *Artif Cells, Nanomedicine, Biotechnol.* 45 (4) (2017) 833–842.
- [44] K. Kinnunen, A. Kauppinen, N. Piippo, A. Koistinen, E. Toropainen, K. Kaarniranta, Cationorm shows good tolerability on human HCE-2 corneal epithelial cell cultures, *Exp. Eye Res.* 120 (2014) 82–89.
- [45] C. Pole, H. Ameri, Fundus autofluorescence and clinical applications, *J. Ophthalmic Vis. Res.* 16 (3) (2021) 432–461.
- [46] M. Koutsovti, A. Siamidi, P. Pavlou, M. Vlachou, Recent advances in the excipients used for modified ocular drug delivery, *Mater* 14 (15) (2021) 4290.
- [47] A. Vedadghavami, C. Zhang, A.G. Bajpayee, Overcoming negatively charged tissue barriers: drug delivery using cationic peptides and proteins, *Nano Today* 34 (2020) 100898.
- [48] N. Sharma, P. Madan, S. Lin, Effect of process and formulation variables on the preparation of parenteral paclitaxel-loaded biodegradable polymeric nanoparticles: a co-surfactant study, *Asian J. Pharm. Sci.* 11 (3) (2016) 404–416.
- [49] A.T. Ojo, C. Ma, P.I. Lee, Elucidating the effect of crystallization on drug release from amorphous solid dispersions in soluble and insoluble carriers, *Int. J. Pharm.* 591 (2020) 120005.
- [50] A. Khosa, S. Reddi, R.N. Saha, Nanostructured lipid carriers for site-specific drug delivery, *Biomed. Pharmacother.* 103 (2018) 598–613.
- [51] Z. Huang, C. Ma, M. Wu, X. Li, C. Lu, X. Zhang, et al., Exploring the drug-lipid interaction of weak-hydrophobic drug loaded solid lipid nanoparticles by isothermal titration calorimetry, *J. Nanoparticle Res.* 22 (1) (2020) 1–14.
- [52] A. Hutin, N. Lima, F. Lopez, M. Carvalho, Stability of silica nanofluids at high salinity and high temperature, *Powders* 2 (1) (2022) 1–20.
- [53] G. Zoubari, S. Staufenbiel, P. Volz, U. Alexiev, R. Bodmeier, Effect of drug solubility and lipid carrier on drug release from lipid nanoparticles for dermal delivery, *Eur. J. Pharm. Biopharm.* 110 (2017) 39–46.
- [54] X. Li, Q. Li, C. Zhao, Zero-order controlled release of water-soluble drugs using a marker pen platform, *ACS Omega* 6 (21) (2021) 13774–13778.
- [55] M. Luciano, Mathematical models of drug release, in: *Strategies to Modify the Drug Release from Pharmaceutical Systems*, Woodhead Publishing, 2015, pp. 63–86.
- [56] F. Shafiei, M. Ghavami-Lahiji, T.S.J. Kashi, F. Najafi, Drug release kinetics and biological properties of a novel local drug carrier system, *Dent. Res. J.* 18 (2021) 94.
- [57] J.H. Ahn, H. Do Kim, S.M. Abuzar, J.Y. Lee, S.E. Jin, E.K. Kim, et al., Intracorneal melatonin delivery using 2-hydroxypropyl- β -cyclodextrin ophthalmic solution for granular corneal dystrophy type 2, *Int. J. Pharm.* 529 (1–2) (2017) 608–616.
- [58] V. Andrés-Guerrero, P. Alarma-Estrany, I.T. Molina-Martínez, A. Peral, R. Herrero-Vanrell, J. Pintor, Ophthalmic formulations of the intraocular hypotensive melatonin agent 5-MCA-NAT, *Exp. Eye Res.* 88 (3) (2009) 504–511.
- [59] A. Crooke, F. Huete-Toral, B. Colligris, J. Pintor, The role and therapeutic potential of melatonin in age-related ocular diseases, *J. Pineal Res.* 63 (2) (2017) e12430.
- [60] S.S. Chrai, T.F. Patton, A. Mehta, J.R. Robinson, Lacrimal and instilled fluid dynamics in rabbit eyes, *J. Pharmaceut. Sci.* 62 (7) (1973) 1112–1121.
- [61] A. Subrizi, E.M. del Amo, V. Korzhikov-Vlakh, T. Tennikova, M. Ruponen, A. Urtili, Design principles of ocular drug delivery systems: importance of drug payload, release rate, and material properties, *Drug Discov. Today* 24 (8) (2019) 1446–1457.
- [62] W. Yang, L. Wang, E.M. Mettenbrink, P.L. Deangelis, S. Wilhelm, Nanoparticle toxicology, *Annu. Rev. Pharmacol. Toxicol.* 61 (2021) 269–289.
- [63] W. Zhang, X. Li, T. Ye, F. Chen, S. Yu, J. Chen, et al., Nanostructured lipid carrier surface modified with Eudragit RS 100 and its potential ophthalmic functions, *Int. J. Nanomed.* 9 (2014) 4315.
- [64] D.N. Hu, J.E. Roberts, Melatonin inhibits growth of cultured human uveal melanoma cells, *Melanoma Res.* 7 (1) (1997) 27–31.
- [65] E.A. Carreño, Alberto Avp, C.A.M. de Souza, H.L. de Mello, A. Henriques-Pons, L. A. Alves, Considerations and technical pitfalls in the employment of the MTT assay to evaluate photosensitizers for photodynamic therapy, *Appl. Sci.* 11 (6) (2021) 2603.
- [66] H. Zhao, L. Wu, G. Yan, Y. Chen, M. Zhou, Y. Wu, et al., Inflammation and tumor progression: signaling pathways and targeted intervention, *Signal Transduct. Targeted Ther.* 6 (1) (2021) 1–46.
- [67] N. Singh, D. Baby, J. Rajguru, P. Patil, S. Thakkannavar, V. Pujari, Inflammation and cancer, *Ann. Afr. Med.* 18 (3) (2019) 126.
- [68] S. Liao, J.Z. Wang, E. Zagarella, P. Paulus, N.H.Q.H. Dang, T. Rawling, et al., An update on inflammation in uveal melanoma, *Biochimie* 212 (2023) 114–122.
- [69] J. Blasiak, R.J. Reiter, K. Kaarniranta, Melatonin in retinal physiology and pathology: the case of age-related macular degeneration, *Oxid. Med. Cell. Longev.* 2016 (2016) 6819736.
- [70] P.H. Sande, D. Dorfman, D.C. Fernandez, M. Chianelli, A.P. Domínguez Rubio, A. M. Franchi, et al., Treatment with melatonin after onset of experimental uveitis attenuates ocular inflammation, *Br. J. Pharmacol.* 171 (24) (2014) 5696–5707.
- [71] J. Meng, B. Lin, S. Huang, Y. Li, P. Wu, F. Zhang, et al., Melatonin exerts anti-angiogenic and anti-inflammatory effects in alkali-burned corneas, *Ann. Transl. Med.* 10 (8) (2022), 432–432.
- [72] S.P. Balguri, G.R. Adelli, S. Majumdar, Topical ophthalmic lipid nanoparticle formulations (SLN, NLC) of indomethacin for delivery to the posterior segment ocular tissues, *Eur. J. Pharm. Biopharm.* 109 (2016) 224–235.
- [73] A.M. Mohsen, Cationic polymeric nanoparticles for improved ocular delivery and antimycotic activity of terconazole, *J. Pharmaceut. Sci.* 111 (2) (2022) 458–468.
- [74] A.R. Fernandes, L.B. Vidal, E. Sánchez-López, T. dos Santos, P.L. Granja, A.M. Silva, et al., Customized cationic nanoemulsions loading triamcinolone acetonide for corneal neovascularization secondary to inflammatory processes, *Int. J. Pharm.* 623 (2022) 121938.
- [75] R. Yan, L. Xu, Q. Wang, Z. Wu, H. Zhang, L. Gan, Cyclosporine A nanosuspensions for ophthalmic delivery: a comparative study between cationic nanoparticles and drug-core mucus penetrating nanoparticles, *Mol. Pharm.* 18 (12) (2021) 4290–4298.
- [76] P. Nirbhavane, L. Moksha, G. Sharma, T. Velpandian, B. Singh, O.P. Katare, Cationic nano-lipidic carrier mediated ocular delivery of triamcinolone acetonide: a preclinical investigation in the management of uveitis, *Life* 13 (4) (2023) 1057.